Intraflagellar transport-20 coiled-coil domain mediates the channelrhodopsins trafficking to the cilia in *Chlamydomonas reinhardtii*

Alka Kumari and Suneel Kateriya*

Laboratory of Optobiotechnology, School of Biotechnology, Jawaharlal Nehru University, New Delhi, India.

*To whom correspondence should be addressed.

Corresponding authors' e-mail: skateriya@jnu.ac.in

†ORCID identifiers: S.K. 0000-0001-5428-4297

Abstract

The primary cilium is a microtubule-based structure essential for cellular signaling, whose assembly and function depend on targeted delivery of cargo via intraflagellar transport (IFT). Intraflagellar transport-20 (IFT20), a unique IFT-B component, localizes to both the Golgi and cilia, suggesting a central role in ciliary trafficking. We analyzed the IFT20-mediated trafficking (CrIFT20) of photoreceptor channelrhodopsin-1 (ChR1) in the cilia of *Chlamydomonas reinhardtii* using an integrative approach that combines computational and experimental methods. The sequence homology and structural modelling reveal a conserved C-terminal coiled-coil domain in IFT20, supporting its canonical function in IFT-B assembly. Furthermore, the heterologous expression and spectroscopic characterization demonstrate that recombinant CrIFT20 is structurally stable and undergoes GTP-dependent structural rearrangements. This is consistent with our docking analyses, which show that human Arf4 homolog in *C. reinhardtii*, small ARF-related GTPase (CrARFA1A) interacts with the conserved coiled-coil region of CrIFT20 in a GTP-binding interface. Interaction network mapping and structural docking supported a conserved mechanism in which CrIFT20 couples ciliary trafficking with IFT-B and BBSome components, such as BBS1, for precise delivery of ciliary membrane cargo. The IFT81 and BBS1 mutants of *C. reinhardtii* mislocalizes IFT20-ChR1 complex in cilia and disrupts photoreceptor distribution, as supported by structural models that reveal the corresponding adaptor-cargo interfaces. Our results identify CrIFT20 as an essential adaptor linking IFT-B complex, CrARFA1A-mediated membrane trafficking, and BBSome-dependent sorting to direct ChR1 localization within the cilia of *Chlamydomonas*. These findings expand the mechanistic understanding of photoreceptor delivery in algae, and reveal a conserved role of IFT20 in photoreceptor trafficking, illuminating how coordinated adaptor, motor, and cargo selection maintain the polarized architecture of the cilia.

Keywords: Intraflagellar transport-20, Channelrhodopsin-1, Ciliary trafficking, Coiled-coil domain, *Chlamydomonas reinhardtii*.

1. Introduction

The primary cilium is a non-motile, microtubule-based projection that functions as a sensory antenna for extracellular signals. Its structure and function rely on precisely regulated trafficking pathways that direct membrane proteins and signaling molecules from the cytoplasm and Golgi to the ciliary compartment (Hsiao et al., 2012; Sánchez & Dynlacht, 2016). This delivery is governed by specific targeting motifs, such as the VxPx sequence in rhodopsin, and by coordinated vesicular transport orchestrated through Rab GTPases, Arfs, and the intraflagellar transport (IFT) machinery (Mukhopadhyay, 2017; Schou et al., 2015). When any of these processes are disrupted, core signaling pathways break down, leading to a diverse group of developmental and sensory disorders known as ciliophaties (Satir et al., 2010).

Central to ciliary assembly and homeostasis is the IFT system, a multi-subunit transport machinery composed of two major complexes (Mirvis et al., 2018). The IFT-B complex (Morthorst et al., 2018) drives kinesin-2-mediated anterograde transport to the ciliary tip, whereas the IFT-A complex enables dynein -2-mediated retrograde transport of IFT particles and cargo for reuse (Sánchez & Dynlacht, 2016; Sung & Leroux, 2013). Among IFT-B components, IFT20 is particularly distinctive, unlike other IFT proteins, as it localizes not only to the basal body and ciliary transition zone but also to the Golgi complex (Follit et al., 2008). This strategic positioning enables IFT20 to couple post-Golgi vesicular trafficking with the entry of cargo into the cilia. In addition, Arf GTPase and Rab GTPases mediate ciliary trafficking (Hanke-Gogokhia et al., 2016). Arf4 initiates cargo sorting at the Golgi by recognizing ciliary targeting signals and promoting vesicle budding (Wang et al., 2017). Rab11 and Rab8 GTPases then drive the movement, docking, and fusion of IFT20-marked vesicles at the periciliary membrane through the Rab11-Rabin8-Rab8 cascade (Hanke-Gogokhia et al., 2016; Ward et al., 2011). At this point of convergence, IFT20 is incorporated into the IFT-B complex, where it helps coordinate the entry, sorting, and anterograde transport of membrane and axonemal cargo along the axoneme via kinesin-2. Disruption at any of these stages, whether in Arf/Rab regulation, IFT20 adaptor function, or IFT complex integrity, results in defective ciliary assembly or mislocalized signaling receptors, contributing to sensory deficits and ciliopathies. Working alongside the IFT machinery is the BBSome, an octameric protein complex that acts as a critical adaptor for ciliary membrane trafficking (Nozaki et al., 2018). Mutations in BBSome components impair trafficking efficiency, causing IFT proteins and membrane receptors to accumulate abnormally at the ciliary tip, as observed in Bardet-Biedl Syndrome (BBS). The core BBSome subunits (BBS-1, 2, 7, 9) form the structural backbone of

the complex and mediate membrane protein-cargo interactions, whereas the accessory subunits (BBS-4, 5, 8, 18) facilitate basal-body targeting and membrane association (Jenkins & Hernandez-Hernandez, 2015). Notably, BBS1 and BBS10 account for a significant proportion of BBS cases in human populations (Muller et al., 2010). Structural studies have revealed that the IFT20-IFT38 module of the IFT-B complex interacts with BBS1, BBS2, and BBS9, forming a functional docking interface at the ciliary base or on IFT trains. This interface facilitates the regulated transfer of GPCRs and other signaling cargo between the IFT machinery and the BBSome, ensuring precise loading and unloading at the ciliary base and tip (Wang et al., 2022). This IFT-BBSome motor coordination is conserved. In the unicellular alga *Chlamydomonas reinhardtii*, analogous trafficking pathways direct the proper delivery and retention of bacteriorhodopsin-type rhodopsins within the flagellar membrane, where they mediate light-dependent phototaxis (Awasthi et al., 2016). However, the role of IFT20 in the trafficking of channelrhodopsins remains poorly understood.

To address this gap, we investigated the role of IFT20 in ciliary trafficking of channelrhodopsins in *C. reinhardtii*. Previous studies suggest that Channelrhodopsin-1 (CrChR1) relocates between the eyespot and flagella in a light-dependent manner, whereas Channelrhodopsin-2 is exclusively localized to the eyespot and basal body under similar conditions (Awasthi et al., 2016). Building on this framework, we performed a comprehensive bioinformatic, biochemical, and cell-biological assessment CrIFT81 and CrBBS1 mutant strains of *C. reinhardtii*. In this study, we focus solely on the IFT20-mediated ciliary distribution of channelrhodopsins. Our findings reveal that heterologously expressed CrIFT20 protein exhibits GTP-dependent fluorescence quenching and undergoes specific secondary-structure transitions. Furthermore, cellular characterization in mutant strains of *Chlamydomonas* demonstrates that perturbation of CrIFT81 and CrBBS1 function leads to mislocalization of the IFT20 and CrChR1 complex within defined ciliary sub-compartments. Overall, the findings reveal a conserved role of IFT20 in channelrhodopsins ciliary trafficking, advancing our understanding of photoreceptor transport in *Chlamydomonas*.

2. Materials and methods

2.1 Bioinformatic analysis of IFT20 homologs

The IFT20 protein sequences were obtained from the NCBI (https://www.ncbi.nlm.nih.gov/) and JGI Genome Portal (https://jgi.doe.gov/) by performing pBLAST searches against the non-redundant database. Domain architecture was analyzed using the CDART tool (Geer, 2002).

The multiple protein sequence homology analysis was performed using the ClustalW program and visualized by BioEdit (http://www.mbio.ncsu.edu/bioedit/bioedit.html). The identification of conserved motifs within IFT20 sequences was carried out using the Multiple Expectation Maximization for Motif Elicitation (MEME) Suite (MEME version 5.5.8) (Bailey et al., 2015). Motifs showing strong statistical support (E-value: 1×10^{-5}) were selected for downstream analyses, and their significance was determined based on the associated E-values. An analysis of the secondary structure was performed using the CFSSP (Chou and Fasman Secondary Structure Prediction Server) online tool, available via the ExPASy server. The DISOPRED3 (Disorder Prediction) and MEMSAT-SVM (membrane helix-interaction) signal peptide search was performed by PSIPRED (McGuffin, 2000). Phylogenetic analysis of IFT20 proteins was performed in MEGA11 (Tamura et al., 2021) using 1000 bootstrap replicates. Pairwise distances were calculated with the JTT model (Jones et al., 1992), and initial trees were generated using the Neighbor-Joining and BioNJ methods. These preliminary topologies were then evaluated to identify the tree with the highest log-likelihood score.

2.2 Protein-protein interaction network prediction for photoreceptor trafficking in *Chlamydomonas*.

Core IFT-BBSome and ancillary sequences were obtained from JGI and NCBI and subjected to protein-protein interaction (PPI) analysis using STRING v11, based on multisource evidences (Szklarczyk et al., 2019). Interaction networks were subsequently visualized using Cytoscape v3.10.3 (Shannon et al., 2003).

2.3 Structural modelling of IFT20 homologs and evaluation of predicted interaction interfaces

The tertiary structures of IFT20 homologs were predicted individually using the AlphaFold Server (https://alphafoldserver.com/welcome). Model quality was assessed with the SAVES validation suite (https://saves.mbi.ucla.edu/). Structural visualization and cross-species superposition were carried out in PyMOL v3.1 (https://www.pymol.org/). The protein structures for CrIFT20, CrARFA1A, CrBBS1, CrChR1, and CrIFT81 were predicted using the AlphaFold-Multimer workflow on the AlphaFold server (Evans et al., 2021). FASTA sequences were submitted using default settings, and five models were generated for each complex. The highest-confidence mode was selected for further analysis. All predicted complexes were visualized in PyMOL v3.1 (https://www.pymol.org/), and interaction interfaces were examined based on residue contact maps, complementary surface geometry, and electrostatic surface

potentials. These models were used to infer putative adaptor-cargo interaction regions among CrIFT20, CrARFA1A, CrBBS1, CrChR1, and CrIFT81.

2.4 Heterologous expression and affinity purification of recombinant CrIFT20 proteins

The synthesized CrIFT20 coding sequence was sub-cloned into the pET21a(+) vector and expressed in *E. coli* BL21 (λDE3). An overnight-grown culture was inoculated into 500 mL Terrific Broth medium (TB) with 100 µg/mL ampicillin and grown at 37 °C and 200 rpm to an OD_{600} of 0.6–0.8. After chilling on ice for 45 minutes, culture induction was carried out with 0.3 mM IPTG and grown at 16 °C for 48 hours. Cells were harvested (3,500×g, 10 min, 4°C), resuspended in PBS buffer containing lysozyme (0.5 mg/mL) and PMSF (0.2 mM), and lysed by sonication (50% amplitude, 10 s on/off, 10 min). The lysates were subjected to centrifugation (13,000 × g, 60 min, 4 °C), filtered (0.45 µm), and the resulting supernatant was loaded onto a pre-equilibrated Ni-NTA IMAC column with PBS (150 mM NaCl, 10 mM sodium phosphate, pH 7.2). After binding and washing, His-tagged CrIFT20 was eluted with 250 mM imidazole. Purified protein samples were subjected to separation on a 12% SDS-PAGE gel and then transferred to a nitrocellulose membrane under cold-transfer conditions (350 mA, 90 min). Membranes were blocked with 5% milk in PBST and incubated with anti-His primary antibodies (1:5000), followed by HRP-conjugated secondary antibodies. Signal detection was carried out using enhanced chemiluminescence (ECL). The workflow for recombinant protein expression and purification was adapted from established protocols. (Wang, 2018; Taschner, 2016).

2.5 Fluorescence spectroscopy of recombinant CrIFT20

Purified CrIFT20 obtained from Ni-NTA IMAC chromatography was buffer-exchanged into PBS (pH 7.5) prior to fluorescence analysis. Fluorescence emission spectra were recorded for CrIFT20 both before and after titration with increasing concentrations of GTP. Fluorescence spectra were obtained with a Cary Varian Eclipse fluorimeter (Varian, Victoria, Australia). The protein samples were excited at a wavelength of 292 nm, and the emission was collected in the range of 300 to 400 nm. Background fluorescence from buffer controls was subtracted from all measurements. Data analysis was carried out according to the procedures outlined in the referenced study (dos Santos Rodrigues et al., 2023).

2.6 Circular dichroism spectroscopy recombinant CrIFT20

Purified recombinant CrIFT20 was analyzed by far-UV circular dichroism (190–260 nm), using PBS as the buffer control. CD spectral changes were monitored following the addition of increasing GTP concentrations. Measurements were performed on a Jasco J-815 spectrometer (Jasco, Tokyo, Japan) equipped with a 250 W xenon lamp, using a 1 mm path-length cuvette, a scanning speed of 50 nm.min-1, and a bandwidth of 0.5 nm. Each spectrum represents the average of three scans, and buffer background spectra were subtracted from all datasets.

2.7 *Chlamydomonas* culture, protein extraction, and immunoblotting

All *Chlamydomonas* strains were sourced from the *Chlamydomonas* Resource Center (https://www.chlamycollection.org/). The wild-type strains were grown in standard TAP (Tris-Acetate-Phosphate) medium, whereas mutant strains were cultivated in TAP medium with an addition of 0.1 g/L arginine. Cultures were maintained at 22 °C under a specific light/dark cycle of 14 hours of light followed by 10 hours of darkness, with continuous shaking at 110 rpm to ensure even aeration and nutrient distribution (Catalan, 2025) . After 5 to 6 days of cultivation, cultures were collected at an optical density (OD_{800}) of approximately 0.6 by centrifugation at 5000 rpm for 10 minutes. The pelleted cells were resuspended in PBS containing 0.1% protease inhibitor cocktail (PIC) and subjected to lysis through sonication at 30% amplitude, using 8-second on/off intervals for a total of 20 cycles. The lysates were then clarified via centrifugation at 13,000 rpm for 15 minutes, and the supernatant obtained was combined with Laemmli buffer and heated at 65 °C for 30 minutes. Proteins were separated on a 12% SDS-PAGE gel and examined through immunoblotting using a CrIFT20-specific antibody.

2.8 Cellular co-immunolocalization of CrIFT20 and ChR1

Coverslips were rinsed and treated with a solution of 0.1 mg/mL poly-L-lysine. *Chlamydomonas* cells were placed onto the poly-L-lysine-coated coverslips and allowed to rest for 15 minutes at ambient temperature. The coverslips with *C. reinhardtii* cells were then exposed to a freshly made 3.7% paraformaldehyde solution in PBS for about 15 minutes. Coverslips were subsequently placed in ice-cold absolute ethanol at -20 °C for 20 minutes, with gentle agitation occurring intermittently. After the fixation process, cells were rehydrated in PBS that had 250 mM NaCl, and then they were washed four times with PBST (PBS supplemented with 0.5% Triton X-100). The permeabilized *Chlamydomonas* cells were then

incubated overnight with a freshly diluted primary antibody of CrIFT20 (1:250) and ChR1-Ct (1:250) at 4°C. In Western blot analysis, the ChR1-Ct antibody immune-detects both Channelrhodopsins-1 and 2. However, the study focusses on CrChR1 trafficking in cilia, where CrChR2 is known to be absent (Awasthi et al., 2016). After that, the cells were washed four times, 2 minutes each, with PBST and PBS, then incubated at 37 °C for one hour with Alexa Fluor-conjugated secondary antibodies (Invitrogen, USA): anti-goat Alexa-488 and anti-rabbit Alexa-547. Again, after washing with PBST and then PBS, the coverslips were affixed onto acid-washed glass slides using SlowFade® Gold antifade reagent (Molecular Probes, Invitrogen, USA) positioned in an inverted manner for slide visualization (Lewis et al., 2024). Samples were visualized using an Olympus Fluoview 1000 confocal microscope (Lewis et al., 2024; Lechtreck, 2013).

3. Results and Discussion

3.1 Phylogenetic and sequence homology analysis reveal a conserved functional core of IFT20 in ciliary trafficking

Comparative sequence homology and secondary structure analyses of IFT20 homologs revealed that the C-terminal coiled-coil domain is highly conserved, consistent with its established role in intraflagellar transport complex assembly (Baker et al., 2003). In contrast, the N-terminal region displays marked sequence variation and comprises β-strands linked by a flexible loop (Fig. 1A), a configuration likely contributing to species-specific modulation of IFT20 function and its interactions within the ciliary transport system. Motif analysis further identified discrete, conserved sequence elements across homologs, detected through expectation-maximization algorithms that quantify motif enrichment and position-specific conservation (Fig. 1A). These motifs define critical interaction interfaces required for engaging intraflagellar transport components or adaptor proteins involved in ciliary trafficking. Notably, a conserved YEFI motif (Y111–E118–F124–I129) emerged as a key determinant mediating IFT20's interaction with the WD40 domain of the autophagy-related protein ATG16 (Boukhalfa et al., 2021). Phylogenetic reconstruction further supports this pattern of structural constraint and molecular divergence. Chlorophyte sequences create a well-supported clade, suggesting that the IFT20 structure in algae has stayed consistent among flagellated green lineages (Fig. 1B). Streptophyte homologs, including those from early land plants, form a distinct cluster, consistent with functional divergence associated with terrestrial adaptation. Oomycete IFT20 proteins group together in a well-supported (bootstrap 100), lineage-specific

clade, reflecting the adaptation of the IFT pathway within this heterokont group. Metazoan homologs form a separate basal branch, consistent with an early evolutionary split of the ciliary transport machinery in animals (Merchant et al., 2007). Among all groups, Chlorophyta exhibits the highest retention of the ancestral IFT20 configuration (Fig. 1B), consistent with the conserved molecular features required for ciliary transport in *Chlamydomonas*. Together, the combined sequence alignment and phylogenetic evidence demonstrate that IFT20 retains a highly conserved core essential for its canonical role in IFT-B assembly, while the flanking regions accumulate lineage-specific variability that may support specialized regulatory functions. The close clustering of *Chlamydomonas* with other chlorophytes supports the use of *C. reinhardtii* as a tractable model for studying ancestral features of IFT20-mediated ciliary trafficking.

3.2 A conserved coiled-coil module stabilizes the IFT20 structure

Recombinant CrIFT20 was heterologously expressed in *E. coli*. Bacterial cultures carrying the expression construct were lysed, and the clarified lysates were purified using immobilized metal affinity chromatography (IMAC), which enabled the selective enrichment of His-tagged CrIFT20. The purified fractions were resolved on SDS–PAGE. A prominent band of ~15 kDa was observed (Supplementary Figure S1A), matching the predicted size of full-length CrIFT20 (Taschner et al., 2016). The gel was used for western blotting with an anti-His antibody. Elution fractions E1 to E5 displayed a strong ~15 kDa signal, confirming that the purified protein corresponds to the His-tagged CrIFT20, thereby validating the successful purification. Integrative structural modelling coupled with biophysical validation revealed that IFT20 proteins maintain a deeply conserved architectural core across eukaryotes. Cross-species superposition of predicted IFT20 protein structures demonstrated near-perfect alignment of the C-terminal coiled-coil region (Fig. 2A). Despite substantial divergence within the N-terminal segment, consistent with its role as a rigid interaction platform required for stable incorporation into the IFT-B scaffold and for maintaining IFT train architecture. Intrinsic fluorescence spectroscopy of recombinant CrIFT20 revealed an emission maximum at ~330 nm (Fig. 2B), indicating burial of tryptophan residues within a hydrophobic core and supporting formation of a compactly folded tertiary state. Far-UV circular dichroism spectra showed prominent minima at 208 and 222 nm (Fig. 2C), confirming a strongly α-helical signature in agreement with the predicted structural models. De novo quantitative secondary-structure profiling across IFT20's homologs further demonstrated uniformly elevated helical content (76–93%)

(Supplementary Table S1). In contrast, β-strand and turn content varied in a lineage-dependent manner, suggesting that structural plasticity is restricted to peripheral regions not directly involved in IFT-B complex assembly. Together, these data indicate that IFT20 possesses a highly conserved helical core that is evolutionarily constrained to preserve its architectural and scaffolding functions within ciliary transport systems, while allowing modular divergence in non-core segments that may underlie lineage-specific tuning of IFT20 protein dynamics (Finetti et al., 2022).

3.3 GTP-modulated structural change and docking interactions reveal structural regulation of recombinant CrIFT20

To define the molecular machinery involved in channelrhodopsin-1 (ChR1) trafficking within the cilia of *C. reinhardtii*, we first mapped the core and ancillary flagellar proteins that co-associate with ChR1. This analysis was performed using a curated protein-protein interaction (PPI) network specific to *C. reinhardtii* (Supplementary Figure S2A). This comprehensive PPI integrates four major curated clusters, defining vesicle-mediated transport proteins and intraflagellar transport (IFT) components. We next identified the highest-confidence interactors (Supplementary Figure S2B). The resulting top-interacting protein network revealed a densely interconnected module comprising canonical IFT-B components (IFT57, IFT80, IFT88, IFT172, IFT74), membrane-trafficking GTPases (Arl3, RABG1, RABA1, YKT6, ARFA1), and BBSome subunits (BBS1, BBS5, BBS7) (Hanke-Gogokhia et al., 2016; Pazour et al., 2002; Boegholm et al., 2023; Wang et al., 2017). High-ranked nodes corresponded to proteins with established roles in ciliary membrane trafficking.

These findings support the central positioning of IFT20 at the interface between IFT-B assembly and GTPase-mediated vesicle-associated transport pathways (Lechtreck et al., 2009; Wingfield et al., 2018; Follit et al., 2008). To evaluate how CrIFT20 couples with small GTPase for ciliary trafficking of proteins, we performed an integrative docking study of CrIFT20 with the small GTPase CrARFA1A in its active, GTP-bound state. Active Arf4-GBF1 (Guanine Nucleotide Factor 1) at the Golgi/Trans-Golgi network engages with the ciliary cargo rhodopsin, defining a regulatory node in ciliary membrane trafficking (Ward et al., 2011; Wang et al., 2017). CrIFT20 model docked onto an equivalent surface of active ARA41A, positioning the conserved C-terminal coiled-coil adjacent to the GTP-Mg^{2+} pocket (Fig. 3A). The local interface is enriched in polar and electrostatic contacts surrounding the switch regions of CrARFA1A, suggesting a potential GTP-sensitive binding geometry. We next examined

whether GTP binding modulates the conformation of CrIFT20. Intrinsic fluorescence spectroscopy further showed progressive quenching of the tryptophan emission maximum upon addition of GTP (Fig. 3B), consistent with burial of aromatic residues and a tighter tertiary packing state. The far-UV circular dichroism measurements revealed that increasing the concentrations of GTP induced subtle but reproducible changes in ellipticity around 208–222 nm (Fig. 3C). These shifts indicate alterations in α-helical packing rather than global unfolding. The magnitude of quenching is proportional to GTP concentration, supporting a nucleotide-dependent structural rearrangement. These results identify CrIFT20 as an interaction hub linking the IFT-B complex to CrARFA1A-mediated membrane trafficking. This demonstrates that GTP modulates IFT20's structural state, potentially tuning its engagement with trafficking regulators during early steps of ciliary cargo sorting

3.4 Cellular co-localization of IFT20 and ChR1 in *Chlamydomonas reinhardtii*

IFT20 is a key adaptor protein involved in the sorting of ciliary membrane proteins, dynamically shuttling between the Golgi complex, basal body, and cilium (Follit et al., 2006). For understanding the molecular and cellular function of IFT20 in *C. reinhardtii.* We performed immunofluorescence detection using a CrIFT20-specific antibody in the wild-type *C. reinhardtii* strain CC125, which revealed that IFT20 is prominently localized within the ciliary compartment (Fig. 4A). The staining appears as punctate green fluorescence throughout the cilium, consistent with previous reports of IFT20 localization along the basal body and ciliary axoneme. Co-immunostaining with ChR1, a known ciliary photoreceptor protein (Awasthi et al., 2016) demonstrated significant spatial overlap with IFT20 in the merged fluorescence images, clearly indicating that IFT20 and ChR1 co-localize in the cilia (Fig. 4A). Further, immunoblotting was performed to evaluate the expression and specificity of IFT20 protein in *C. reinhardtii* CC124 (wild-type) cells. Total cell lysate was prepared and followed by immunoblotting using a CrIFT20-specific antibody (Fig. 4B). The resulting blot revealed a prominent and distinct band at approximately 15 kDa. The same blot probed with pre-immune serum at the same dilution failed to detect any corresponding band, indicating a lack of non-specific binding and confirming the high specificity of the antibody for CrIFT20 (Fig. 4B). The molecular weight and banding pattern are consistent with prior reports, further validating antibody performance and confirming that the detected protein is indeed IFT20. These findings demonstrate, at the molecular level, that IFT20 is robustly expressed in *C. reinhardtii.* This co-localization supports a functional interaction in which IFT20 likely facilitates the targeted

trafficking and proper localization of photoreceptors, such as ChR1, within the flagella of *C. reinhardtii*. To understand the mechanistic framework of the interaction between IFT20-ChR1, in silico structural modelling was performed. The predicted model defined a putative interaction interface between the coiled-coil architecture of IFT20 and the cytoplasmic regions of ChR1, supporting a direct physical association (Fig. 4C).

3.5 CrIFT81 and CrBBS1 mutations disrupt intracellular trafficking of the IFT20-ChR1 complex in *C. reinhardtii*

3.5.1 Loss of CrIFT81 alters IFT20-ChR1 localization in cilia

IFT81 serves as a tubulin-binding adaptor within the IFT-B complex (Kubo et al., 2016) ,and together with IFT74, forms an unconventional GAP that modulates RabL2 activity during early intraflagellar transport (Boegholm et al., 2023). This study unveils a novel aspect of intraflagellar transport (IFT)-dependent cargo delivery in *C. reinhardtii* through analysis of the IFT81 mutant. In wild-type cells, the IFT20–ChR1 complex is robustly localized at the basal body and distributed along the ciliary length, demonstrating efficient IFT-mediated trafficking into the cilium and supporting normal channelrhodopsin-1 function in photoreception and ciliary signaling. However, as depicted in the figure, the IFT81 mutant (CC5863/ift81-1mt) exhibits altered localization pattern: green (IFT20) and red (ChR1) signals are confined to discrete sub-ciliary regions, with a striking absence along the cilium, indicating that defective IFT81 disrupts the normal directional trafficking of the complex (Fig. 5A). Intriguingly, the merge panel reveals prominent co-localization of IFT20-ChR1 at the eyespot, a subcellular compartment critical for phototactic responses. While no prior evidence has documented IFT-modeled cargo delivery to this organelle. This observation introduces a previously unrecognized pathway for cargo trafficking to the eyespot, implicating IFT machinery, and specifically IFT81, as a potential regulator beyond cilia. Accompanying structural modelling reveals the predicted interaction surfaces between the coiled-coil domain of IFT81 and the cytoplasmic regions of ChR1, as well as the coiled-coil domain of IFT20 (Fig. 5B & C). These interfaces support a model in which IFT81 and IFT20 function as cargo adaptors that assist in the delivery and stable localization of photoreceptor proteins within the flagellar membrane. Supporting evidence from recent studies suggests that mutations in IFT particle components can cause the mislocalization of rhodopsins in both the eyespot and the flagella. This supports the idea that IFT-dependent mechanisms help regulate the dynamic distribution of sensory photoreceptors between these compartments, potentially in a light-dependent

manner. However, the specific effects of IFT81 disruption on eyespot photoreceptor trafficking and signal processing remain unresolved and will require detailed mechanistic and structural investigations.

3.5.2 CrBBS1 mutation results in asymmetrical ciliary distribution of CrChR1

BBSome mutations restrict the trafficking of ciliary membrane proteins by impairing their entry and exit. Although CC4371/bbs1mt forms full-length flagella with normal IFT, the loss of BBS1 disrupts the export of key signaling proteins, such as phospholipase D, resulting in defective phototaxis (Lechtreck et al., 2009). A Core Complex of BBS Proteins Cooperates with the GTPase Rab8 to promote ciliary membrane Biogenesis (Nachury et al., 2007). This study demonstrates that in the BBS1 mutant strain (CC-4371/*bbs1mt*), IFT20 (green) and ChR1 (red) signals are predominantly confined to the distal tip of the trans cilium. The merged yellow signal indicates accumulation and co-localization of the IFT20–ChR1 complex in this region (Fig. 6A). Unlike wild-type cells, which show symmetrical distribution of ChR1 along the *cis- and trans*-flagellum, the *bbs1* mutant displays a restricted asymmetrical localization pattern, reflecting defective trafficking. These results demonstrate that the loss of BBS1 disrupts the bidirectional transport of CCrChR1, causing the abnormal retention of the IFT20-ChR1 complex at the ciliary tip, which affects the phototaxis signalling of Chlamydomonas reinhardtii. Furthermore, *in silico* structural modelling predicts the surface interaction interface between BBS1 and ChR1, as well as IFT20. The interface typically involves the docking of IFT20s between its central coiled-coil and N-terminal regions and surface grooves on the β-propeller and N-terminal arm of BBS1 (Fig. 6B & C). This configuration facilitates IFT20 recruitment into the BBSome macromolecule assembly and positions it as an adaptor linking vesicle-associated transport factors to cargo recognition. Overall, these findings underscore the crucial role of BBS1 along with IFT20 in maintaining the polarized distribution and dynamic trafficking of photoreceptor-associated proteins in *C. reinhardtii*.

4. Conclusions and future perspectives

This study identifies *Chlamydomonas reinhardtii* IFT20 as a conserved adaptor that mediates trafficking of CrChR1. The integrative multi-scale analysis demonstrates that CrIFT20 possesses a highly conserved coiled-coil core essential for its architectural role in IFT-B assembly and persistent trafficking functions within eukaryotic cilia. Comparative sequence, structural, and phylogenetic investigations reveal lineage-specific variability in peripheral

regions, but strong evolutionary conservation is maintained in the functional domain required for interaction with key transport machinery. The conserved coiled-coil module, verified through recombinant expression of CrIFT20 and fluorescence and circular dichroism spectroscopy, showed that CrIFT20 retains a deeply conserved C-terminal coiled-coil domain and is strongly linked to efficient ciliary protein transport and sorting. Cellular analyses further showed that IFT20 robustly localizes within the ciliary compartment and co-localizes with the photoreceptor channelrhodopsin-1 (CrChR1), as supported by structural models that predict a direct binding interface. These observations identify IFT20 as a cargo-proximal module that facilitates the targeted delivery of sensory receptors to the ciliary membrane. Loss of CrIFT81 disrupts the IFT20–ChR1 complex and leads to its unexpected accumulation at the eyespot, suggesting an unrecognized IFT-linked pathway for photoreceptor redistribution between cellular compartments. In contrast, BBS1 deficiency results in asymmetric retention of the IFT20-ChR1 complex at the distal ciliary tip, consistent with defective BBSome-mediated export and impaired phototactic signaling. Structural modelling of IFT20–BBS1 interactions supports a mechanistic role for IFT20 in coupling the IFT-B scaffold to BBSome-dependent membrane retrieval. Together, these findings identify IFT20 as a central adaptor that integrates IFT-B, Arf-dependent membrane trafficking, and BBSome-mediated cargo sorting to maintain the polarized distribution of channelrhodopsin-1 proteins in *Chlamydomonas*. This work provides a mechanistic framework for understanding how sensory receptors are dynamically partitioned between the cilium and associated photoreceptive organelles, highlighting IFT20 as a key molecular node that coordinates these trafficking pathways in *Chlamydomonas reinhardtii*.

CRediT authorship contribution statement

Suneel Kateriya: Conceptualisation, Data curation and Methodology, Supervision, Validation, Funding acquisition, Writing-review and editing. **Alka Kumari:** Formal analysis, Investigation, Writing-original draft, Methodology.

Funding sources

We are thankful to ANRF/SERB, Government of India for granting EEQ/2023/000398 research project.

Declaration of competing interest

The authors declare no competing interests.

Acknowledgements

The research grant, EEQ/2023/000398 from ANRF/SERB, is duly acknowledged. Alka Kumari is the recipient of the Senior Research Fellowship from UGC (JRF), Govt. of India. We gratefully acknowledge Dr Shilpa Mohanty for the critical review of the article.

Data availability

Data is available on request.

References

1) Awasthi, M., Ranjan, P., Sharma, K., Veetil, S. K., & Kateriya, S. (2016). The trafficking of bacterial type rhodopsins into the *Chlamydomonas* eyespot and flagella is IFT mediated. *Scientific Reports*, *6*. https://doi.org/10.1038/srep34646
2) Bailey, T. L., Johnson, J., Grant, C. E., & Noble, W. S. (2015). The MEME Suite. *Nucleic Acids Research*, *43*(W1), W39–W49. https://doi.org/10.1093/nar/gkv416
3) Boegholm, N., Petriman, N. A., Loureiro-López, M., Wang, J., Vela, M. I. S., Liu, B., Kanie, T., Ng, R., Jackson, P. K., Andersen, J. S., & Lorentzen, E. (2023). The IFT81-IFT74 complex acts as an unconventional RabL2 GTPase -activating protein during intraflagellar transport. *The EMBO Journal*, *42*(18). https://doi.org/10.15252/embj.2022111807
4) Boukhalfa, A., Roccio, F., Dupont, N., Codogno, P., & Morel, E. (2021). The autophagy protein ATG16L1 cooperates with IFT20 and INPP5E to regulate the turnover of phosphoinositides at the primary cilium. *Cell Reports*, *35*(4). https://doi.org/10.1016/j.celrep.2021.109045
5) Catalan, R. E., Fragkopoulos, A. A., Girot, A., Lorenz, M., & Bäumchen, O. (2025). Preparation, maintenance and propagation of synchronous cultures of photoactive *Chlamydomonas* cells. *Nature Protocols*, *20*(8), 2125–2150. https://doi.org/10.1038/s41596-024-01135-3
6) dos Santos Rodrigues, F. H., Delgado, G. G., Santana da Costa, T., & Tasic, L. (2023). Applications of fluorescence spectroscopy in protein conformational changes and

intermolecular contacts. *BBA Advances*, *3*. https://doi.org/10.1016/j.bbadva.2023.100091

7) Evans, R., O'Neill, M., Pritzel, A., Antropova, N., Senior, A., Green, T., Žídek, A., Bates, R., Blackwell, S., Yim, J., Ronneberger, O., Bodenstein, S., Zielinski, M., Bridgland, A., Potapenko, A., Cowie, A., Tunyasuvunakool, K., Jain, R., Clancy, E., … Hassabis, D. (2021). *Protein complex prediction with AlphaFold-Multimer*. https://doi.org/10.1101/2021.10.04.463034
8) Finetti, F., Onnis, A., & Baldari, C. T. (2022). IFT20: An Eclectic Regulator of Cellular Processes beyond Intraflagellar Transport. In *International Journal of Molecular Sciences* (Vol. 23, Issue 20). MDPI. https://doi.org/10.3390/ijms232012147
9) Follit, J. A., San Agustin, J. T., Xu, F., Jonassen, J. A., Samtani, R., Lo, C. W., & Pazour, G. J. (2008). The Golgin GMAP210/TRIP11 anchors IFT20 to the Golgi complex. *PLoS Genetics*, *4*(12). https://doi.org/10.1371/journal.pgen.1000315
10) Follit, J. A., Tuft, R. A., Fogarty, K. E., & Pazour, G. J. (2006). The Intraflagellar Transport Protein IFT20 Is Associated with the Golgi Complex and Is Required for Cilia Assembly. V. *Molecular Biology of the Cell*, *17*, 3781–3792. https://doi.org/10.1091/mbc.E06
11) Geer, L. Y., Domrachev, M., Lipman, D. J., & Bryant, S. H. (2002). CDART: Protein homology by domain architecture. *Genome Research*, *12*(10), 1619–1623. https://doi.org/10.1101/gr.278202
12) Hanke-Gogokhia, C., Wu, Z., Gerstner, C. D., Frederick, J. M., Zhang, H., & Baehr, W. (2016). Arf-like protein 3 (ARL3) regulates protein trafficking and ciliogenesis in mouse photoreceptors. *Journal of Biological Chemistry*, *291*(13), 7142–7155. https://doi.org/10.1074/jbc.M115.710954
13) Hsiao, Y. C., Tuz, K., & Ferland, R. J. (2012). Trafficking in and to the primary cilium. In *Cilia* (Vol. 1). https://doi.org/10.1186/2046-2530-1-4
14) Jenkins, D., & Hernandez-Hernandez, V. (2015). Advances in the understanding of the BBSome complex structure and function. *Research and Reports in Biology*, 191. https://doi.org/10.2147/rrb.s65700
15) Jones, D. T., Taylor, W. R., & Thornton, J. M. (1992). The rapid generation of mutation data matrices from protein sequences. In *CABIOS* (Vol. 8, Issue 3). https://academic.oup.com/bioinformatics/article/8/3/275/193076
16) Kubo, T., Brown, J. M., Bellve, K., Craige, B., Craft, J. M., Fogarty, K., Lechtreck, K. F., & Witman, G. B. (2016). Together, the IFT81 and IFT74 N-termini form the main

module for intraflagellar transport of tubulin. *Journal of Cell Science*, *129*(10), 2106–2119. https://doi.org/10.1242/jcs.187120

17) Lechtreck, K. F. (2013). In vivo imaging of IFT in Chlamydomonas flagella. In *Methods in Enzymology* (Vol. 524, pp. 265–284). Academic Press Inc. https://doi.org/10.1016/B978-0-12-397945-2.00015-9

18) Lechtreck, K. F., Johnson, E. C., Sakai, T., Cochran, D., Ballif, B. A., Rush, J., Pazour, G. J., Ikebe, M., & Witman, G. B. (2009). The Chlamydomonas reinhardtii BBSome is an IFT cargo required for export of specific signaling proteins from flagella. *Journal of Cell Biology*, *187*(7), 1117–1132. https://doi.org/10.1083/jcb.200909183

19) Lewis, T. R., Castillo, C. M., Klementieva, N. V., Hsu, Y., Hao, Y., Spencer, W. J., Drack, A. V., Pazour, G. J., & Arshavsky, V. Y. (2024). Contribution of intraflagellar transport to compartmentalization and maintenance of the photoreceptor cell. *Proceedings of the National Academy of Sciences of the United States of America*, *121*(34). https://doi.org/10.1073/pnas.2408551121

20) Merchant, S. S., Prochnik, S. E., Vallon, O., Harris, E. H., Karpowicz, S. J., Witman, G. B., Terry, A., Salamov, A., Fritz-Laylin, L. K., Maréchal-Drouard, L., Marshall, W. F., Qu, L. H., Nelson, D. R., Sanderfoot, A. A., Spalding, M. H., Kapitonov, V. V., Ren, Q., Ferris, P., Lindquist, E., … Zhou, K. (2007). The Chlamydomonas genome reveals the evolution of key animal and plant functions. *Science*, *318*(5848), 245–251. https://doi.org/10.1126/science.1143609

21) Mirvis, M., Stearns, T., & Nelson, W. J. (2018). Cilium structure, assembly, and disassembly regulated by the cytoskeleton. In *Biochemical Journal* (Vol. 475, Issue 14, pp. 2329–2353). Portland Press Ltd. https://doi.org/10.1042/BCJ20170453

22) Morthorst, S. K., Christensen, S. T., & Pedersen, L. B. (2018). Regulation of ciliary membrane protein trafficking and signalling by kinesin motor proteins. In *FEBS Journal* (Vol. 285, Issue 24, pp. 4535–4564). Blackwell Publishing Ltd. https://doi.org/10.1111/febs.14583

23) Muller, J., Stoetzel, C., Vincent, M. C., Leitch, C. C., Laurier, V., Danse, J. M., Hellé, S., Marion, V., Bennouna-Greene, V., Vicaire, S., Megarbane, A., Kaplan, J., Drouin-Garraud, V., Hamdani, M., Sigaudy, S., Francannet, C., Roume, J., Bitoun, P., Goldenberg, A., … Dollfus, H. (2010). Identification of 28 novel mutations in the Bardet-Biedl syndrome genes: The burden of private mutations in an extensively heterogeneous disease. *Human Genetics*, *127*(5), 583–593. https://doi.org/10.1007/s00439-010-0804-9

24) Nachury, M. V., Loktev, A. V., Zhang, Q., Westlake, C. J., Peränen, J., Merdes, A., Slusarski, D. C., Scheller, R. H., Bazan, J. F., Sheffield, V. C., & Jackson, P. K. (2007). A Core Complex of BBS Proteins Cooperates with the GTPase Rab8 to Promote Ciliary Membrane Biogenesis. *Cell*, *129*(6), 1201–1213. https://doi.org/10.1016/j.cell.2007.03.053

25) Nozaki, S., Katoh, Y., Kobayashi, T., & Nakayama, K. (2018). BBS1 is involved in retrograde trafficking of ciliary GPCRs in the context of the BBSome complex. *PLoS ONE*, *13*(3). https://doi.org/10.1371/journal.pone.0195005

26) Pazour, G. J., Baker, S. A., Deane, J. A., Cole, D. G., Dickert, B. L., Rosenbaum, J. L., Witman, G. B., & Besharse, J. C. (2002). The intraflagellar transport protein, IFT88, is essential for vertebrate photoreceptor assembly and maintenance. *Journal of Cell Biology*, *157*(1), 103–113. https://doi.org/10.1083/jcb.200107108

27) Sánchez, I., & Dynlacht, B. D. (2016). Cilium assembly and disassembly. In *Nature Cell Biology* (Vol. 18, Issue 7, pp. 711–717). Nature Publishing Group. https://doi.org/10.1038/ncb3370

28) Satir, P., Pedersen, L. B., & Christensen, S. T. (2010). The primary cilium at a glance. In *Journal of Cell Science* (Vol. 123, Issue 4, pp. 499–503). https://doi.org/10.1242/jcs.050377

29) Shannon, P., Markiel, A., Ozier, O., Baliga, N. S., Wang, J. T., Ramage, D., Amin, N., Schwikowski, B., & Ideker, T. (2003). Cytoscape: A software Environment for integrated models of biomolecular interaction networks. *Genome Research*, *13*(11), 2498–2504. https://doi.org/10.1101/gr.1239303

30) Sung, C. H., & Leroux, M. R. (2013). The roles of evolutionarily conserved functional modules in cilia-related trafficking. *Nature Cell Biology*, *15*(12), 1387–1397. https://doi.org/10.1038/ncb2888

31) Szklarczyk, D., Gable, A. L., Lyon, D., Junge, A., Wyder, S., Huerta-Cepas, J., Simonovic, M., Doncheva, N. T., Morris, J. H., Bork, P., Jensen, L. J., & Von Mering, C. (2019). STRING v11: Protein-protein association networks with increased coverage, supporting functional discovery in genome-wide experimental datasets. *Nucleic Acids Research*, *47*(D1), D607–D613. https://doi.org/10.1093/nar/gky1131

32) Tamura, K., Stecher, G., & Kumar, S. (2021). MEGA11: Molecular Evolutionary Genetics Analysis Version 11. *Molecular Biology and Evolution*, *38*(7), 3022–3027. https://doi.org/10.1093/molbev/msab120

33) Taschner, M., Weber, K., Mourão, A., Vetter, M., Awasthi, M., Stiegler, M., Bhogaraju, S., & Lorentzen, E. (2016). Intraflagellar transport proteins 172, 80, 57, 54, 38, and 20 form a stable tubulin-binding IFT -B2 complex. *The EMBO Journal*, *35*(7), 773–790. https://doi.org/10.15252/embj.201593164

34) Wang, J., Fresquez, T., Kandachar, V., & Deretic, D. (2017). The Arf GEF GBF1 and Arf4 synergize with the sensory receptor cargo, rhodopsin, to regulate ciliary membrane trafficking. *Journal of Cell Science*, *130*(23), 3975–3987. https://doi.org/10.1242/jcs.205492

35) Wang, J., Zhu, X., Wang, Z., Li, X., Tao, H., & Pan, J. (2022). Assembly and stability of IFT-B complex and its function in BBSome trafficking. *IScience*, *25*(12). https://doi.org/10.1016/j.isci.2022.105493

36) Wang, Q., Taschner, M., Ganzinger, K. A., Kelley, C., Villasenor, A., Heymann, M., Schwille, P., Lorentzen, E., & Mizuno, N. (2018). Membrane association and remodeling by intraflagellar transport protein IFT172. *Nature Communications*, *9*(1). https://doi.org/10.1038/s41467-018-07037-9

37) Ward, H. H., Brown-Glaberman, U., Wang, J., Morita, Y., Alper, S. L., Bedrick, E. J., Gattone, V. H., Deretic, D., & Wandinger-Ness, A. (2011). A conserved signal and GTPase complex are required for the ciliary transport of polycystin-1. *Molecular Biology of the Cell*, *22*(18), 3289–3305. https://doi.org/10.1091/mbc.E11-01-0082

38) Wingfield, J. L., Lechtreck, K. F., & Lorentzen, E. (2018). Trafficking of ciliary membrane proteins by the intraflagellar transport/BBSome machinery. In *Essays in Biochemistry* (Vol. 62, Issue 6, pp. 753–763). Portland Press Ltd. https://doi.org/10.1042/EBC20180030

Figures

(A)
C.elegans_IFT20
H.sapiens_IFT20
C.reinhardtii_IFT20
K.nitens_IFT20
T.brucei_IFT20
Motif I
Motif II
Motif III
coiled-coil domain
β-Strand
loop region

(B)

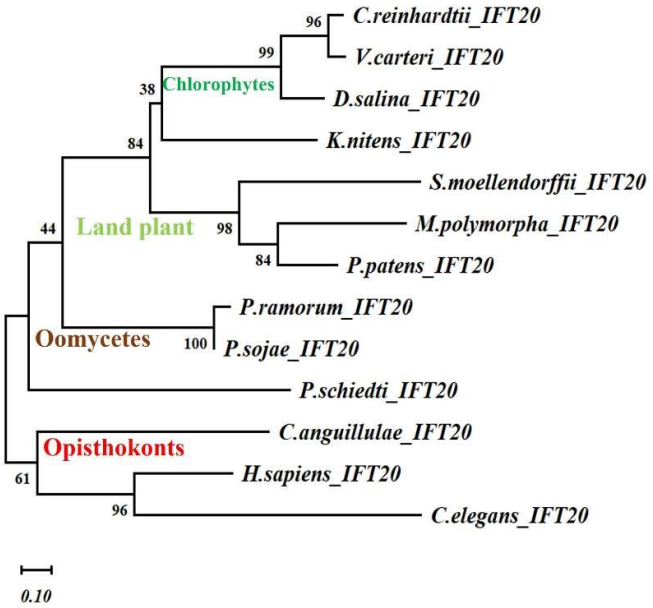

Fig. 1. Sequence conservation and evolutionary relationships of IFT20 homologs. (A) Multiple sequence alignment of IFT20 protein sequences from diverse organisms. Conserved residues are highlighted by blue color. The alignment highlights strong conservation across the IFT20 sequences. A schematic representation of the predicted secondary structural elements is shown above the alignment: α-helices (blue bars), β-strands (yellow arrows), and loop regions (grey), indicating structural conservation. MEME (Multiple Expectation Maximization for Motif Elicitation) finds three discrete motif regions that is shown in the figure. The height of each letter reflects the conservation of residue. The organisms selected are: *Homo sapiens, Trypanosoma brucei, Chlamydomonas reinhardtii, Klebsormidium nitens, Caenorhabditis elegans.* (B) Alignment of IFT20 protein sequences was carried out using ClustalW in MEGA11. The tree was analyzed using the Maximum likelihood method and the Jonas-Taylor-Thorton model with 1000 bootstrap replicates. Evolutionary analyses were conducted using MEGA 11 software.

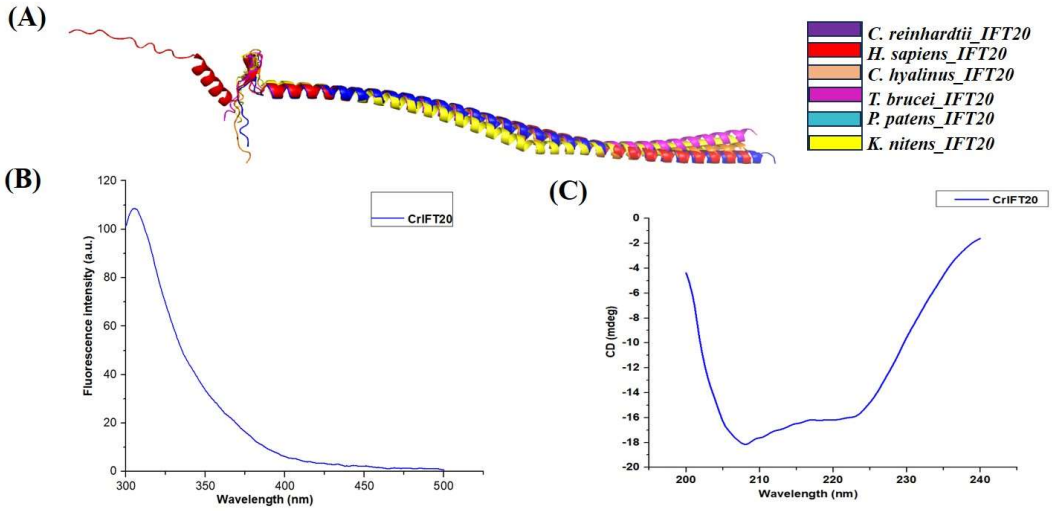

Fig. 2. Structural comparison and spectroscopic characterization of recombinant CrIFT20 by intrinsic fluorescence and CD spectroscopy. (A) Structural superposition of IFT20 sequences from *Chlamydomonas reinhardtii*, Homo *sapiens*, *Chlamydomonas hyalinus*, *Trypanosoma brucei*, *Physcomitrella patens*, and *Klebsormidium nitens*, colour-coded by species. (B) The intrinsic fluorescence emission profile of recombinant CrIFT20 protein was recorded between 300-500 nm upon excitation at 280 nm. The single emission peak indicates the typical tryptophan fluorescence signature. (C) Circular dichroism (CD) spectrum of recombinant CrIFT20, with dominant negative peaks characteristic of α-helical secondary structure.

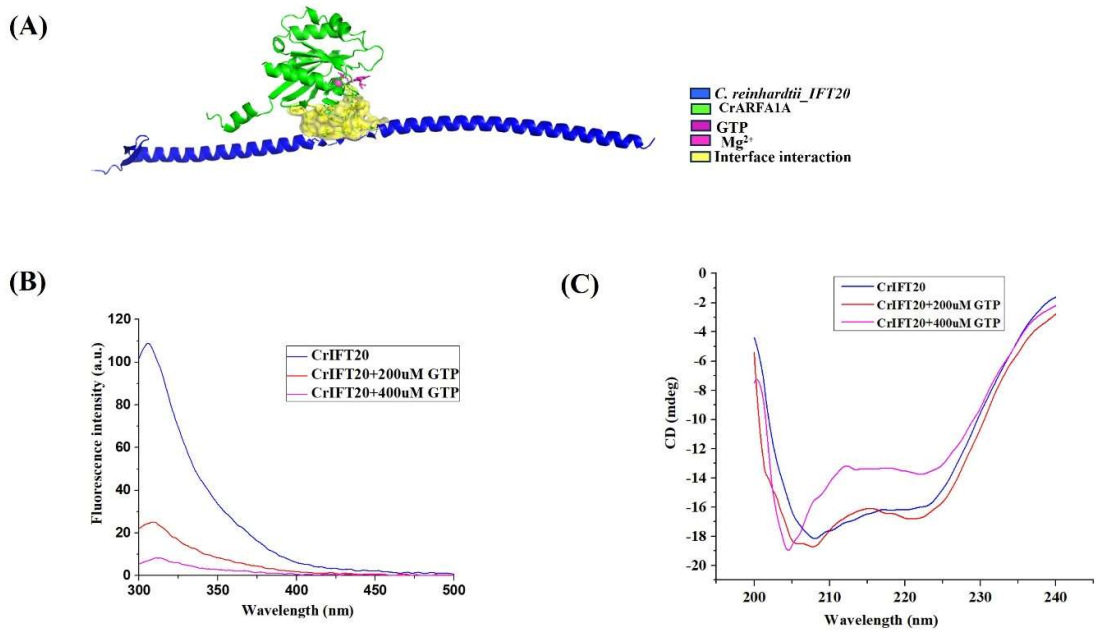

Fig. 3. Molecular docking and GTP-dependent spectroscopic characterization of recombinant CrIFT20. (A) Structural docking of CrIFT20(blue) with CrARFA1A (orange), with the predicted interaction interface highlighted (yellow). CrARFA1A interacts with the CrIFT20 coiled-coil near the GTP-Mg^{2+} pocket. (B) Intrinsic fluorescence spectroscopy of recombinant CrIFT20 with increasing GTP concentrations (200 µM and 400 µM), indicating GTP-dependent changes in the local environment of aromatic residues. (C) Circular dichroism (CD) spectra of recombinant CrIFT20 under identical GTP concentration (200 µM and 400 µM), showing alterations in α-helical secondary-structure signatures. (ARFA1A- Small ARF-related GTPase, GTP - Guanosine Triphosphate).

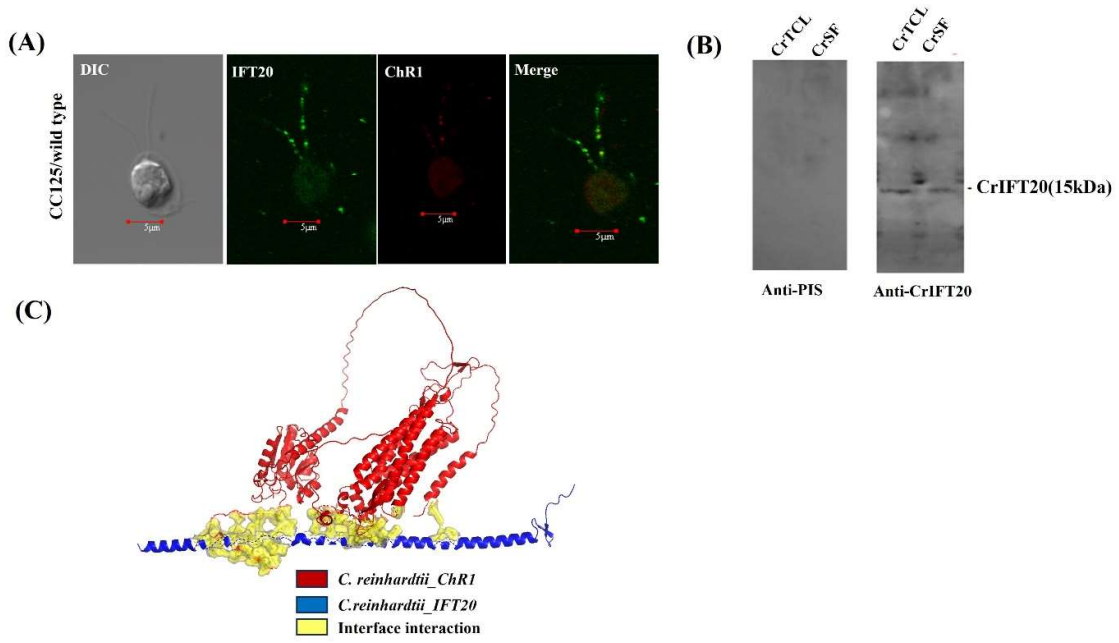

Fig. 4. Co-localization of CrIFT20 with CrChR1 in *Chlamydomonas* wild type CC125 and predicted interaction interface. (A) Immunofluorescence staining of wild-type *Chlamydomonas reinhardtii* (CC125) showing Differential interference contrast (DIC) image with two intact flagella with the cell body, CrIFT20 immunostaining (green), CrChR1 immunostaining (red), and merged channels. CrIFT20 and CrChR1 puncta are both visible within the cilia, with significant spatial overlap in the merged image (yellow), indicating co-localization. Scale bar: 5 µm. (B, C) Immunoblot of total cell lysate (CrTCL) and soluble fraction (CrSF) using anti-CrIFT20 antibody (IB: Anti-CrIFT20, 1:1000 dilution) and a pre-immune serum (PIS) control (IB: Pre-immune serum, 1:1000 dilution). The Anti-CrIFT20 antibody specifically detects a band at the expected size of 15 kDa in the CrTCL and CrSF. Control immunoblot with pre-immune serum shows no corresponding band, confirming the specificity of the anti-CrIFT20 antibody. (C) Structural modelling predicted the interaction interface surface (yellow) between CrIFT20 (blue) and CrChR1 (red). The model positions the conserved coiled-coil region of CrIFT20 in proximity to cytoplasmic domains of CrChR1, supporting a direct physical association that may enable CrIFT20-mediated recruitment or stabilization of CrChR1 during ciliary trafficking. (PIS = pre-immune serum)

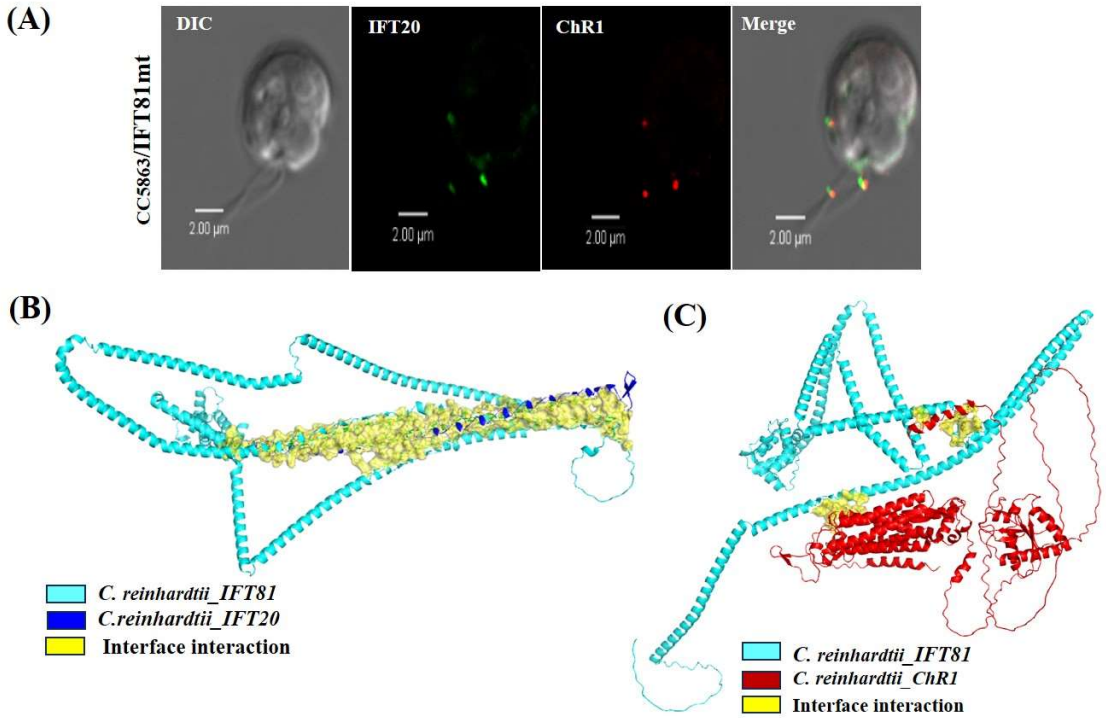

Fig. 5. CrIFT81 mutant alters ciliary localization of the CrIFT20-CrChR1 complex and predicted CrIFT81-CrChR1, CrIFT20-CrIFT81 binding interface interaction. (A) Immunostaining of CC5863/IFT81 mutant cells. Left to right: DIC (cell morphology), CrIFT20 (green), channelrhodopsin-1 (CrChR1, red), and merged images. CrIFT20 and CrChR1signals are confined to discrete sub-ciliary regions, with prominent co-localization at the eyespot and restricted presence along the ciliary shaft. Scale bar: 2 µm. (B-C) Integrative structural models predicted the interaction interfaces (yellow) between CrIFT20 (blue) and CrIFT81 (cyan), as well as between channelrhodopsin-1 (red) and CrIFT81 (cyan). Surface contacts reveal potential adaptor-cargo architecture supporting joint trafficking into the ciliary compartment.

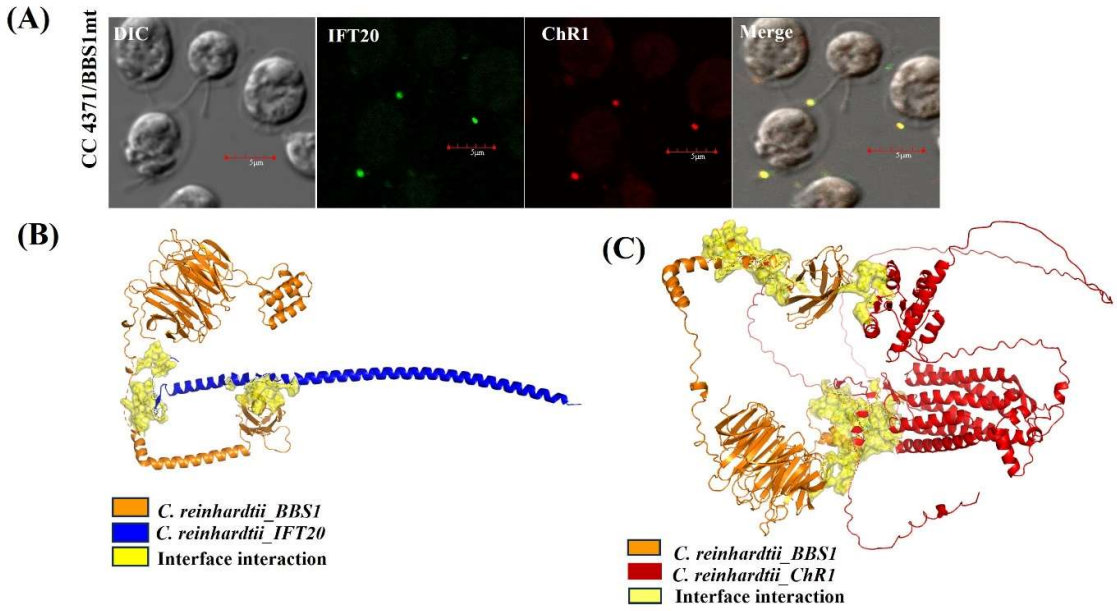

Fig. 6. Mislocalization of the CrIFT20-CrChR1 complex in the CC4371/BBS1 mutant and predicted CrBBS1-CrChR1, CrIFT20-CrChR1 binding interface interaction. (A) Immunofluorescence staining of CC4371/BBS1mt mutant. Left to right: Differential interference contrast (DIC) showing intact flagella. CrIFT20 (green) reveals punctate accumulation predominantly at the distal tip of the *trans* cilium. Channelrhodopsin-1 (CrChR1, red) shows a similarly restricted localization pattern, as shown in the merged image. CrIFT20 and CrChR1 puncta are restricted to the distal tip of the trans cilium, with strong co-localization (yellow) indicating accumulation of the CrIFT20-CrChR1 complex at this site. Unlike wild-type cells, which show symmetrical distribution, the CrBBS1 mutant displays marked asymmetry in protein localization. Scale bar: 5 µm. (B-C) Models predict CrIFT20-CrBBS1 and CrBBS1-CrChR1 interfaces, with CrIFT20 docking on the CrBBS1 β-propeller. Surface mapping shows multiple CrBBS1-CrChR1 contacts across the β-propeller and CrChR1 region.